

Carrier conduction in heterojunction of hydrogenated nanocrystalline silicon with crystal silicon

Wensheng Wei ^{a,*}, Gangyi Xu ^b, Tianmin Wang ^c, W.Z. Shen ^d

^a School of Physics and Electronic information, Wenzhou University, Wenzhou, Zhejiang Province, 325027, China

^b Shanghai Institute of Microsystem and Information Technology, Chinese Academy of Science, Shanghai 200050, China

^c Center of Material Physics and Chemistry, School of Science, Beihang University (BUAA), Beijing 100083, China

^d Laboratory of Condensed Matter Spectroscopy and Optoelectronic Physics, Department of Physics, Shanghai Jiao Tong University, Shanghai 200030, China

Received 25 June 2006; received in revised form 28 August 2006; accepted 29 September 2006

Available online 16 November 2006

Abstract

Phosphorus-doped hydrogenated nanocrystalline silicon (n-type nc-Si:H) film was deposited by plasma enhanced chemical vapor deposition technique on heavy doped p-type crystalline silicon ((p⁺)c-Si) substrate to form heterojunction of (n)nc-Si:H/(p⁺)c-Si. In electrical experiments, both negative resistance in forward current–voltage (*I*–*V*) measurements and current staircases in reverse *I*–*V* experimental data were observed from this structure of (n)nc-Si:H/(p⁺)c-Si at 77 K, which reveals it as a semiconductor heterojunction tunnel diode. The forward current is assigned to interband tunneling, excess and thermionic emission component, respectively. Within reverse bias voltage range from 0 to around –13 V, the reverse current can be ascribed to minority carriers instead of majority carriers tunneling across the depletion layer in heterojunction. Cross reverse applied voltage range from –13 to about –37 V, the reverse current can be attributed to injection of electrons via sequent resonant tunneling through Si nanocrystals into substrate. As further increasing reverse applied voltage, the reverse current can be allocated to carrier avalanche multiplication within amorphous buffer layer region to enhance electron resonant tunneling in nc-Si:H layer.

© 2006 Elsevier B.V. All rights reserved.

PACS: 71.55.Cn; 73.23.Hk; 73.40.-c; 73.61.-r; 73.63.-b

Keywords: Hydrogenated nanocrystalline silicon film; Heterojunction; Carrier conduction mechanism

1. Introduction

Si tunnel diodes have widely been studied in terms of device physics, model, fabrication technology, circuit design and applications for decades [1–3]. Recently, besides artificial nanostructures, resonant tunneling has also been observed in the Si nanocrystals embedded in amorphous matrices. Boeringer and Tsu [4] observed resonant tunneling involving discrete quantum states within Si nanocrystals with *a*-SiO₂ barriers in SiO₂/Si diodes at room temperature. Burr et al. [5] investigated carrier conduction in porous nanoscale Si light emitting devices, of which the carrier transport is controlled by space-charge-limited currents or carrier tunneling through potential barriers.

Hastas et al. [6] reported heterojunction structures of nanocrystalline carbon with crystal silicon and analyzed the current conduction mechanism. Weaver et al. [7] demonstrated the effect of defects on the peak current density and peak to valley current ratio (*PVCR*) of Si-based interband tunneling diodes. Hydrogenated nanocrystalline silicon (nc-Si:H) film that is comprised of Si nanocrystals embedded in hydrogenated amorphous silicon (a-Si:H) matrices, has attracted a great deal of attention due to its potential micro-electronic and photovoltaic device applications as well as interesting physical properties that result from its heterogeneous nature. In our previous work [8], nc-Si:H/c-Si diodes was prepared and current staircases in reverse *I*–*V* measurements due to carrier resonant tunneling was observed, although negative resistance in forward *I*–*V* curve was not detected.

In order to further analyze the carrier transport behavior in nc-Si:H/c-Si, in the present work, phosphorus-doped nc-Si:H

* Corresponding author.

E-mail address: weiwensheng287@sohu.com (W. Wei).

films were deposited by plasma enhanced chemical vapor deposition (PECVD) technique on (p⁺)c-Si substrates, from which electrode/(n)nc-Si:H/(p⁺)c-Si/electrode structures were prepared. Comparing with our previous structure [8], the depletion layer should mainly exist at nc-Si:H side and the barrier height was decreased since the (p⁺)c-Si wafers were used as substrate. Thereby interband tunneling was expected to appear. In addition, from a transmission electronic microscope (TEM) photo of fabricated (n)nc-Si:H/(p⁺)c-Si cross section, an amorphous buffer layer with about 10-nm thickness grown on substrate was found in our present device. This buffer layer can be considered as a large series resistance, which can share the majority of the reverse bias voltage and reduce the potential across the nc-Si:H layer that contains Si nanocrystals. Consequently, the negative applied voltage corresponding to the first current staircase in reverse *I*–*V* curves and the breakdown voltage of the device should increase. Based on the analysis of electrical experiments such as *I*–*V* characteristics, capacitance–voltage (*C*–*V*) profiling, capacitance–frequency (*C*–*f*) curves, deep level transient Fourier spectra (DLTFS) and direct current (DC) conductance experiments, a

tunnel diode of electrode/(n)nc-Si:H/(p⁺)c-Si/electrode was demonstrated while the conduction mechanisms were investigated, as well as a crucial role of the buffer layer was analyzed.

2. Experimental details

A single facet polished (p⁺)c-Si (111) wafer of around 100- μm thickness with an average resistivity of about $5.5 \times 10^{-3} \Omega \text{ cm}$ ($N_A \geq 1.34 \times 10^{19} \text{ cm}^{-3}$) was adopted as substrate material. The (n)nc-Si:H/(p⁺)c-Si structure was prepared with a planer process. Firstly, an around 100-nm thickness SiO₂ layer was prepared by thermal oxidation of substrate wafer at 1293 K. Then the SiO₂ layer was etched and patterned by photolithography to make an array of square holes ($30 \times 30 \mu\text{m}^2$). Secondly, after appropriate treatment, the fresh n-type nc-Si:H film with different ratio of phosphine PH₃ doping in silane (PH₃/SiH₄ in volume percentage, i.e., PH₃/SiH₄ vol%) was separately deposited on the array configuration. Then the outer layer of nc-Si:H film in square holes was removed by etching and photolithography, leaving only around 50-nm thickness phosphorus-doped nc-Si:H layers in hole bottoms. The deposition

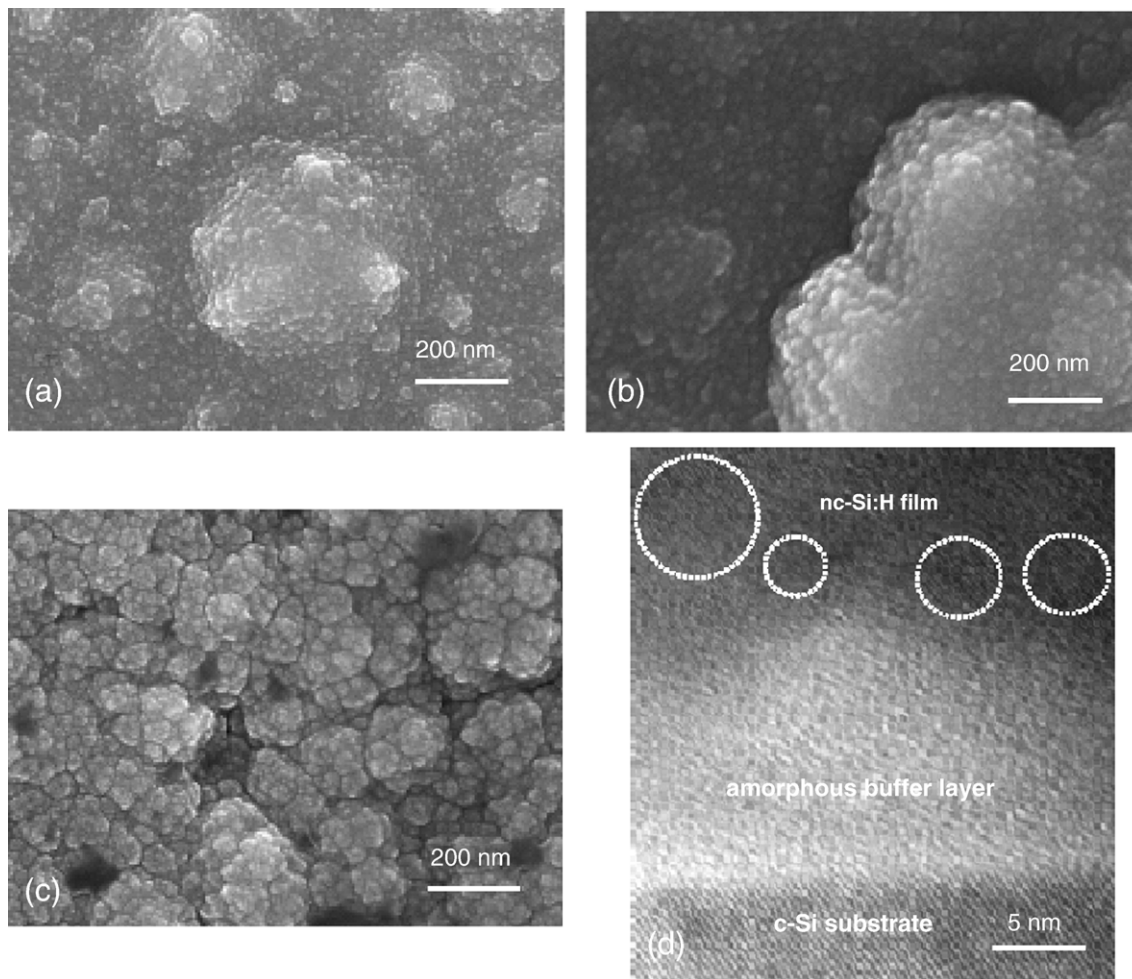


Fig. 1. Plan view SEM images of nc-Si:H samples prepared using doping ratio $C_p = \text{PH}_3/\text{SiH}_4$ vol% of (a) 0.2 vol%, (b) 0.5 vol%, and (c) 1.0 vol%. (d) TEM cross section image of nc-Si:H/c-Si sample prepared using PH_3/SiH_4 doping ratio of 1.0 vol%. Dash circles in (d) highlight the presence of nanocrystals.

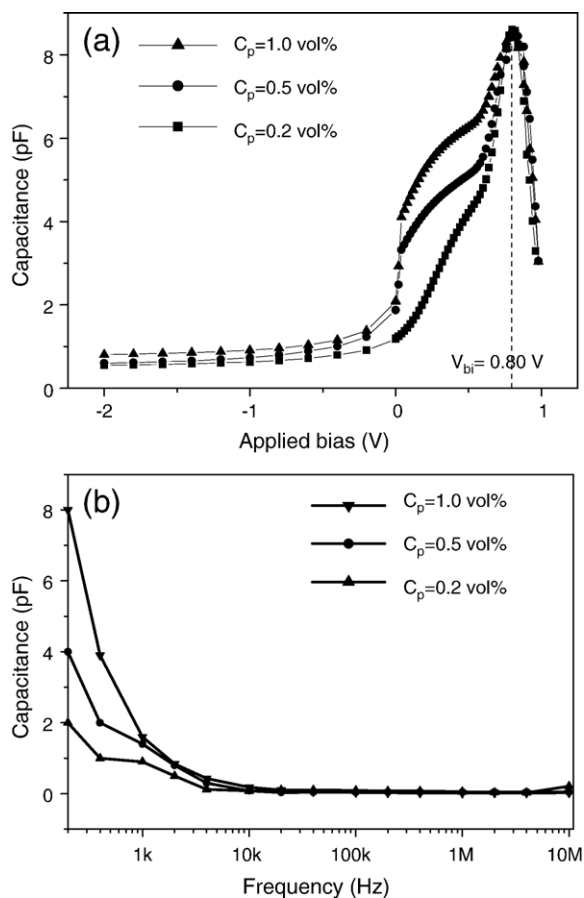


Fig. 2. (a) Capacitance–voltage (C – V) characteristics at 77 K and (b) capacitance–frequency (C – f) curves of electrode/nc-Si:H/c-Si/electrode at 77 K. The dots are experimental data and the connecting lines are guides to eyes.

process was operated in a capacitive coupled radio-frequency (RF of 13.59 MHz) PECVD system aided with negative DC bias stimulation. It is worth specially emphasizing that a strongly hydrogen diluted silane, SiH_4 diluted to 1.00 vol% in H_2 , was used as reactant source gas. Phosphine PH_3 was added into mixed reactant gas to realize doping. The main process parameters, which were also adopted to fabricate a similar nc-Si:H layer on weak doped n-type c-Si in our previous work [8], are listed as following: doping ratio PH_3/SiH_4 vol% of 0.20 ± 0.05 and 0.50 ± 0.05 as well as 1.00 ± 0.05 vol% respectively, substrate temperature of 523 ± 1 K, negative DC bias voltage of -200 ± 2 V, reactant pressure of 100 ± 5 Pa, RF power density of 0.60 ± 0.050 $W\text{ cm}^{-2}$. Subsequently, Au/Cr and Au/Ge alloy as Ohm contact electrodes were prepared by electron-beam evaporation on the sides of substrates and nc-Si:H films respectively. For convenience of electric measurements, finally, the structures of electrode/(n)nc-Si:H/(p⁺)c-Si/electrode were sealed in a ceramic shell with metal contact pads.

The surface morphology of phosphorus-doped nc-Si:H samples was checked by scanning electron microscopy (SEM, JEM-6700F, made in Japan with an operation voltage of 10 kV) and the SEM images were presented in Fig. 1(a), (b) and (c). In order to check microstructures of (n)nc-Si:H/(p⁺)c-Si cross section, the corresponding sample was fabricated by the

following process. Preserving nc-Si:H film while wearing thin c-Si side to about 10 μm with mechanical method. Where after, the nc-Si:H/c-Si structure was placed on a polished metal flat and cut into microscale strips along the direction of film growth. Bearing the orientation of nc-Si:H/c-Si in mind, in one kind of organic acid, the strip was embedded with proper copper at room temperature. Using mechanical method, then this embedded strip was polished to about 1- μm thickness from both sides normal to the direction of film epitaxy. Subsequently, the thickness was diminished to around 150 nm with argon ion bombardment technique. In whole courses, the antioxidation was adopted while the microstructure of (n)nc-Si:H/(p⁺)c-Si was unchanged. The TEM photo for cross section of (n)nc-Si:H/(p⁺)c-Si was taken by transmission electronic microscope (JEM-2010, made in Japan with operation voltage of 200 kV and resolution of 0.19 nm), which is showed in Fig. 1(d).

Using a HP4280A precision LCR meter (L , C and R stands for inductance, capacitance and resistance respectively), the C – V curves of the prepared structure were measured by means of small alternating current (AC) signal (5 mV) of 1 MHz applied to the electrodes at 77 K, as demonstrated in Fig. 2(a). And C – f curves were obtained by a set of multi-frequency LCR meter (HP4274A combination with HP4275A) with small AC signal (5 mV) from 100 Hz to 10 MHz at 77 K, as exhibited in Fig. 2(b).

Testing of deep level transient Fourier spectrum ($DLTFS$) with temperature sweeping manner from 77 to 400 K, was performed by a high sensitivity deep level transient Fourier spectrometer (BIO-RAD-DL8000) at different reverse bias and 0.0 V fixed pulse. The spectra of the sample prepared using PH_3/SiH_4 doping ratio of 0.2 vol% were depicted in Fig. 3 and the experimental results of all devices from $DLTFS$ were listed in Table 1.

To probe the current path among the Si nanocrystals, the dark DC conductance of phosphorus-doped nc-Si:H film, which was grown on glass under the same process condition of (n)nc-Si:H/(p⁺)c-Si prepared using PH_3/SiH_4 doping ratio of 0.2 vol%, was performed using a computer-controlled Keithley 2400 source

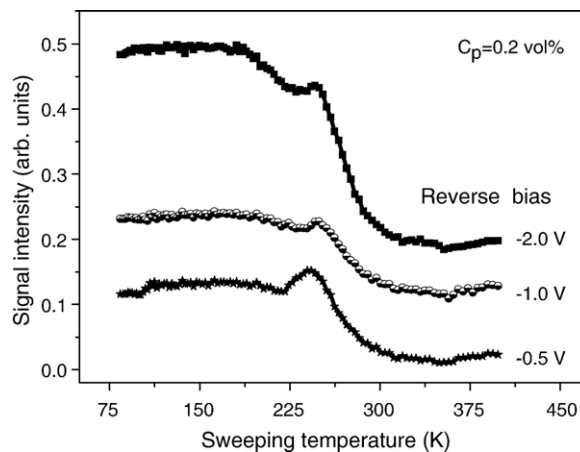


Fig. 3. Deep level transient Fourier spectra ($DLTFS$) of (n)nc-Si:H/(p⁺)c-Si heterojunction prepared using PH_3/SiH_4 doping ratio of 0.2 vol% at different reverse bias of -0.5 V, -1.0 V and -2.0 V and 0.0 V fixed pulse.

Table 1
DLTFS results of three samples at different reverse bias voltage

Sample	Reverse bias V_R/V	$(N_A - N_D) / 10^{19} \text{ cm}^{-3}$	Trap level location E_T/eV	Capture cross section $\Sigma / 10^{-15} \text{ cm}^{-2}$	Trap concentration $N_T / 10^{12} \text{ cm}^{-3}$	$[N_T / (N_A - N_D)] / \%$
0.2 vol%	-0.5				8.11	
	-1.0	1.34	$E_1 = -0.53$	3.0	28.8	$10^{-7} - 10^{-6}$
	-2.0				70.9	
0.5 vol%	-0.5				45.1	
	-1.0	1.34	$E_1 = -0.57$	3.6	71.4	$10^{-6} - 10^{-5}$
	-2.0				149.0	
1.0 vol%	-0.5				51.3	
	-1.0	1.34	$E_1 = -0.61$	4.0	81.9	$10^{-6} - 10^{-5}$
	-2.0				154.4	

meter with an Oxford Optistat^{CF-V} cryostat system within a temperature range from 77 to 300 K, as represented in Fig. 4(a). Also, the dependence of dark conductance on temperature of different doped films, which was grown on glass under the same

process conditions corresponding to the prepared (n)nc-Si:H/(p⁺)c-Si samples, were measured cross temperature range from 20 to 300 K and it is demonstrated in Fig. 4(b). The $I-V$ characteristics of the (n)nc-Si:H/(p⁺)c-Si in Fig. 5(a) and (b) was conducted by a computer-controlled system including HP4140B (PA meter/DC Voltage Source) under 77 K.

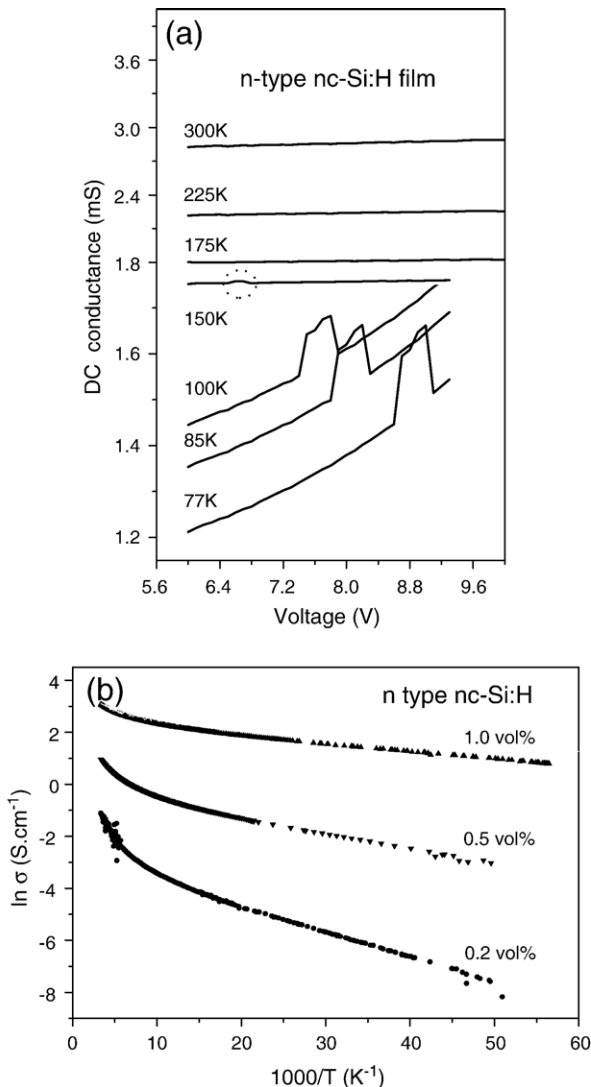


Fig. 4. (a) Dark DC conductance of phosphorus-doped nc-Si:H film prepared using doping ratio PH_3/SiH_4 vol% of 0.2 vol% and (b) temperature dependence of conductance of nc-Si:H films with different doping ratio.

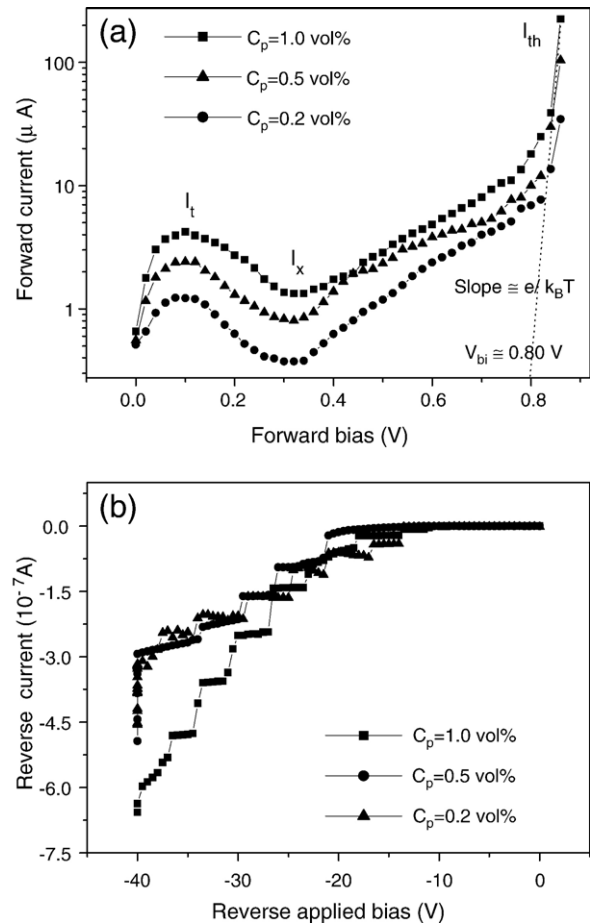


Fig. 5. Current–voltage ($I-V$) characteristics of (n)nc-Si:H/(p⁺)c-Si structures. (a) For forward and (b) reverse $I-V$ measurements. The dots are experimental data and the connecting lines are guides to eyes. Within measured range, I increases dramatically with increasing positive applied voltage V and for the sample prepared using doping ratio PH_3/SiH_4 vol% of 1.0 vol%, the slope of fitting tangent closing to $e/k_B T$ and the built in potential, $V_{bi} \approx 0.8$ V.

3. Results and discussion

3.1. Capacitance–voltage characteristics

One can easily find from the C – V curves in Fig. 2(a) that the capacitance, C , are dramatically varied with the positive applied voltage when this voltage is smaller than built in potential V_{bi} . Also, from this figure one can infer that the structures of electrode/(n)nc-Si:H/(p⁺)c-Si/electrode are single semiconductor/semiconductor heterojunctions, since no peak appears in the curves at zero applied voltage [9,10]. Simultaneously, it can be implied from the shape transition of C – V curves that densities of defect trap in the heterojunction structure increase with increasing doping ratio since the slope for C – f curve decreases with raising doping ratio [11]. This observation coincides with *DLTFS* results in Table 1, from which one can find that trap concentration increases while trap energy level falls from the bottom of a conduction band with the increase of doping ratio due to doping. However, the mean size of nanoparticles remains unchanging with the increase of doping level, which can be interpreted in terms of neglectable influence of low doping level on dilution ratio of SiH₄/H₂ vol% that determines the average size of nanocrystals [12]. One can conclude from the results that only a few dopant atoms form nonradiative deep traps, since both trap concentration N_T and the ratio of N_T to net carrier concentration $N_A - N_D$, i.e., $[N_T/(N_A - N_D)]\%$, are very small. In addition, The *DLTFS* results indicate that the trap belongs to bulk defect in nc-Si:H side of heterojunction [13].

The dependence of barrier capacitance C on effective charge density $\rho(\epsilon_b)$ in the heterojunction can be expressed as [14]:

$$C = k k_0 \rho(\epsilon_s) / [2k k_0 \int_0^{\epsilon_s} \rho(\epsilon) d\epsilon]^{1/2} \quad (1)$$

where k is relative dielectric constant of bulk Si and k_0 is vacuum permittivity, ϵ_s is total barrier height. The expression (1) can be adopted to explain our measurements. As we know, only the trap states whose occupation can be changed within emission time $\tau \leq 1/f$ (f of excited signal frequency) can contribute to $\rho(\epsilon_b)$, namely, to barrier capacitance C . Accordingly, the barrier capacitance C decreases with increasing excited signal frequency f , as shown in Fig. 3(b). On the other hand, the increase of trap concentration with raising doping ratio can be assigned to dopant atom inducing disorder. Therefore, the increase of trap concentration N_T with raising dopants can make C increase with the elevation of doping ratio according to expression (1), as demonstrated in Fig. 3(a). Therefore, the deeper the trap locates at, the faster the capacitance drops down with increasing excited signal frequency, as showed in Fig. 3(b). Furthermore, from Table 1 the *DLTFS* results indicate that monoenergetic trap level is located within the bulk of nc-Si:H layer concomitant with the increase of trap concentration as heightening the doping level [10,11]. The presence of single energy trap level in present coexisted system of Si nanocrystals and amorphous Si:H matrices, can be comprehended as the following: the monoenergetic trap level is terraced on the trap levels with a continuous energy distribution within their band-

gap which consists of deep levels and exponential band tails in amorphous matrices.

3.2. Coulomb-blockade effect

It is worth noting that the shoulders in the C – V curves should be attributed to electron trapping in nanocrystals as quantum dots rather than hole trapping from Coulomb-blockade effect [12]. According to dark *DC* conductance (G) measurements in Fig. 4(a) for one phosphorus-doped nc-Si:H film, the fact of a series of apparent peaks emerge in G – V curves reveals the Coulomb-blockade behavior under 150 K. A peak appears near a bias of 6.6 V at 150 K and towards higher voltage with decreasing temperature until reaching 8.7 V at 77 K. It is well known that such a case can be only detectable from a well-defined current path through well ordered nanocrystals. Furthermore, according to the condition of occurring Coulomb-blockade effect [4,15]:

$$C < \frac{e^2}{2k_B T} \quad (2)$$

where C is single quantum dot capacitance, e the electron charge and k_B the Boltzmann constant. In the present case, the capacitance C is estimated to be smaller than 6.18×10^{-18} F. Accordingly, the average size D of nanocrystals can be evaluated to be less than 9.4 nm by using the spherical capacitor formula $C = 2\pi\epsilon_0\epsilon_r D$, with relative dielectric constant $\epsilon_r \sim 11.9$ of bulk Si and vacuum permittivity ϵ_0 . The value D is fitted with the TEM measurement in Fig. 1(d), from which the nanoparticles with about 5-nm size were naturally embedded in amorphous matrices. For more importance, the Coulomb-blockade energy for the mean size of 5.0 nm of nanocrystals in our experiment can be calculated as about 13 meV according to $E_c = \frac{e^2}{2C}$. It is as significant as the value from Boeringer and Tsu [4] in the average size of 3.0 nm of Si nanocrystals. The error between our result and Tsu's can be presumed to derive from the difference of matrix where the quantum dot is embedded. Accordingly, Coulomb-blockade effect can be considered to play an important role in resonant tunneling conduction in present devices.

3.3. Forward I – V characteristics

When the applied bias voltage to (n)nc-Si:H/(p⁺)c-Si structure is zero, the heterojunction is in thermic equilibrium, the operation current is zero as showed in Fig. 5(a). As increasing positive applied voltage to (n)nc-Si:H/(p⁺)c-Si sample, the formed current can be considered as interband tunneling current I_t [1]. With increasing the positive bias voltage, this current I_t continues to increase till up to the largest peak value I_p at peak voltage V_p , as denoted in Fig. 5(a). It may be assigned to the highest tunnel probability since occupied states in n-type nc-Si:H side coinciding with empty allowed states in (p⁺)c-Si side [16]. Subsequently, with further increasing the positive applied voltage, the conduction band in nc-Si:H side becomes uncrossed with the valence band in (p⁺)c-Si side, the current I_t decreases till to the smallest valley value I_v while the negative resistance can

be clearly observed, as illustrated in Fig. 5(a). It can be attributed to the lack of allowed states of corresponding energies for tunneling. The tunneling current I_t can be expressed as [16]:

$$I_t = I_p(V/V_p)\exp(1-V/V_p) \quad (3)$$

where I_p is peak current and V_p is peak voltage value corresponding to I_p . The current I_t falls till to residual component as increasing the positive applied voltage up to the valley voltage V_v . The residual current is so called excess current I_x , which is considered to be mainly dominated by electrons multistep tunneling from conduction band via localized gap states in forbidden band-gap into valence band [6,7,18]. As one can see from *DLTFS* measurements, the density of trap state increases with raising the doping ratio, it will result in the enhancement of the multistep tunneling probability. Accordingly, the excess current I_x will increase with raising the doping ratio in nc-Si:H side. It is just the result in Fig. 5(a). The excess current I_t can be described as [18]:

$$I_x = I_v \exp[A'(V-V_v)] \quad (4)$$

where V_v is valley voltage and A' is coefficient.

When the positive applied voltage is higher than the valley voltage V_v , the measured current I value increases exponentially with increasing applied voltage V , which indicates that normal diffusion (or thermal) current will be governed as in the case of usually p–n junction semiconductor diode. Using a computer program, a least-square fitting with I – V experimental data (within the range of I increasing dramatically with applied voltage) of the sample prepared using PH_3/SiH_4 doping ratio of 1.0 vol% was performed and showed in Fig. 5(a). The results that the slope of fitting tangent closing to $e/k_B T$ and the built in potential $V_{bi} \cong 0.8$ V were obtained, as displayed in Fig. 5(a). It is obvious that the experimental I – V curves (above the valley voltage) can be simulated by the classical junction rectification model as the empirical relationship [16]:

$$I_{th} = I_0 \exp[AV-1] \quad (5)$$

where I_0 is saturation current and A is coefficient. This current component comes from carrier thermionic emission as so called thermal current I_{th} . Thus the total forward current can be expressed as:

$$I = I_t + I_x + I_{th} \quad (6)$$

The *PVCR* of I_p/I_v shows little dependence on variation of doping in nc-Si:H sides, as plotted in Fig. 5(a). It can be interpreted as the following. On the one hand, the tunneling peak current enhances with decrease of heterojunction barrier height and depletion layer width due to increase of carrier concentration from doping in nc-Si:H layer. On the other hand, the excess current increases with localized density of gap states originating from more dopants. Thus the *PVCR* does weakly vary with doping. As a result, the relative steady *PVCR* in present structures does show difference from that of Si-based interband

tunneling diodes from other researcher groups [7]. The change of *PVCR* in the latter derived from altering of quantum well size and disorder. Furthermore, the measured conductance increases while the slope for curve of temperature dependence of conductivity (namely, conductance activated energy) decreases with heightening dopants under about 100 K, as exhibited in Fig. 4 (b). This can be explained in terms of Fermi energy level shift to the bottom of conduct band in phosphorus-doped nc-Si:H film. One can deduce from these data that the forward current in heterojunction of (n)nc-Si:H/(p⁺)c-Si should be enhanced with heightening doping level in phosphorus-doped nc-Si:H films under the same positive applied voltage, which agreed with the experimental results in Fig. 5(a).

3.4. Reverse I – V characteristics

As showed in Fig. 5(b), with increasing negative applied voltage from 0 to about -13 V, the reverse current I_r is just the order of magnitude of 10^{-10} A, and does weakly depend on electrical field at 77 K. The conduction behavior within this negative applied voltage range can be regarded as tunneling instead of electrical field enhanced electron emission [17]. It can be comprehended in terms of *DLTFS* results. As demonstrated in Table 1 and Fig. 3, the trap concentration N_T increase with enhancing negative bias voltage V_r , which indicates that N_T increases with the depth at nc-Si:H side from interface of nc-Si:H/c-Si [10,11]. Since N_A in (p⁺)c-Si side is larger than N_D in (n)nc-Si:H side, the depletion layer should mainly exist at nc-Si:H side. The depletion layer broadens and leads the trap concentration to increase with heightening reverse applied voltage. The traps act as discrete bulk traps rather than continuously interface traps, since the measured signal peaks fix at a temperature and irrespective to reverse bias V_r , as denoted in Fig. 3. Thereby few localized states coming from discrete bulk traps participate in conducting processes. As a result, little cumulative leakage current increases with increasing the reverse bias voltage. In addition, the reverse current shows weak change with doping level in this reverse applied voltage range as exhibited in Fig. 5 (b). Consequently, one can deduce that the carrier transport within this negative applied voltage range is dominated by tunneling transport, namely, the minority carriers tunnel across the depletion layer in heterojunction rather than that of majority carriers. It is just the tunneling behavior for minority carriers rather than generation–recombination mechanism that leads the reverse current to remain little change in different (n)nc-Si:H/(p⁺)c-Si samples with different phosphorus-doped nc-Si:H layers from about 0 to about -13 V, which is displayed in Fig. 5(b).

However, within higher reverse bias ranging from -13 to about -37 V, the plots of I_r versus V_r demonstrate current staircases at 77 K in Fig. 5(b). This observation indicates that the reverse current is generated from electrons resonant tunneling through the Si nanocrystals. The resonant tunneling behavior can be comprehended as following. In the present structure, an amorphous buffer layer of some 10-nm thickness which is indicated in TEM photo was sandwiched between a (p⁺)c-Si substrate and a n-type nc-Si:H layer. With increasing

negative applied voltage to (n)nc-Si:H/(p⁺)c-Si heterojunction, a majority of potential drop can be presumed to take place across the high resistance amorphous buffer layer and a minority appears across the nc-Si:H layer, while the potential drop across (p⁺)c-Si substrate can be neglected. As one can find from TEM photo for cross section of (n)nc-Si:H/(p⁺)c-Si, Si nanocrystals array along the growth direction in nc-Si:H layer and distribute parallel to (n)nc-Si:H/(p⁺)c-Si interface simultaneously. The quantized energy bands can be formed in these nanocrystals as quantum dots due to quantum sized effect [4,15]. Consequently, when the Fermi energy level in alloy electrode is swept by the applied voltage past a quantum state in nanocrystal, its energy level is shifted by a voltage that was shared by a nanocrystal capacitor. Once the condition for Fermi energy level in alloy electrode alignment with the *n*th quantum state in nanocrystal is satisfied, the current jump which originated from injection of electrons via resonant tunneling through the Si nanocrystals as quantum dots into substrate would be observed. Accordingly, the current staircases can be ascribed to sequent resonant tunneling. Furthermore, from Fig. 1(d) one can speculate that only a few nanocrystals are involved in multi-barrier sequent resonant tunneling. These different nanocrystals would induce a few different current staircases, as presented in Fig. 5(b). In addition, the decrease of a value of negative applied voltage corresponding to the first current staircase with the increase of doping can be attributed to reducing of barrier height, which coincides with observation in Fig. 5(b). From SEM pictures in Fig. 1(a), (b) and (c), the mean size of nanocrystals shows independent on doping, which indicates that quantized energy bands of nanocrystals in different heterojunctions would be almost the same [4]. As a consequence, the number of reverse current staircases and the order of magnitude of reverse current are almost the same in different heterojunctions, as showed in Fig. 5(b).

With raising negative applied voltage beyond -37 V, the reverse current increases sharply as displayed in Fig. 5(b). The phenomenon can be assigned to carrier avalanche multiplication in amorphous buffer layer to enhance electrons resonant tunneling in nc-Si:H layer. As aforementioned, the major potential drop appears across amorphous buffer layer, it is likely to be broken down by carrier avalanche multiplication when the reverse bias exceeds -37 V in present devices. The avalanche current superposes resonant tunneling current so as to enshroud the current steps. Our published work [8] on similar structure without buffer layer focused on the reverse applied voltage range from around -7.0 to -9.0 V where current steps appeared in reverse I - V curves. It is nearly within the applied voltage range where the Coulomb-blockade effect emerging in present samples, as presented in Fig. 4(a). However, the structure with higher threshold voltage in the present work is sandwiched by amorphous buffer layer. This layer can share major reverse bias voltage while reducing the potential drop across nc-Si:H film. As a result, the negative applied voltage corresponding to the first current staircase in present structures is increased. One should note that our present results do not contradict the former [8].

4. Conclusion

A kind of heterojunction of (n)nc-Si:H/(p⁺)c-Si was fabricated and its carrier conduction mechanisms were investigated. The forward current is assigned to interband tunneling, excess and thermionic emission component, respectively. However, within the reverse bias range from 0 to around -13 V, the low reverse current can be attributed to minority carrier tunneling across depletion layer in heterojunction. As increasing reverse applied voltage from -13 to about -37 V, the reverse current can be assigned to injection of electrons via sequent resonant tunneling through Si nanocrystals as quantum dots into substrate. With further increasing negative applied voltage beyond -37 V, the reverse current can be considered as carrier avalanche multiplication to enhance electrons resonant tunneling. It is revealed from differential negative resistance emerging in forward I - V measurements while current jumps appearing in reverse I - V experimental data at 77 K that the resulting structure is a tunnel diode.

Acknowledgements

This work was supported by a Natural Science Foundation of China under Contract No. 50471004 and in part supported by a Natural Science Foundation of Zhejiang province of China under Contract No. Y104457.

The authors would like to acknowledge professor Xiaolong Chen and professor Yuexia Li in the Chinese Academy of Science for their technical help. Also, the authors were grateful to Weidong Xiang and Jingfeng Zhang in Wenzhou University in Zhejiang province of China for their SEM check.

References

- [1] L. Esaki, Rev. Mod. Phys. 46 (1974) 237.
- [2] R. Tsu, Nature 364 (1993) 19.
- [3] J.P. Sun, G.I. Haddad, P. Mazumder, J.N. Schulman, Proc. IEEE 86 (1998) 641.
- [4] D.W. Boeringer, R. Tsu, Phys. Rev., B 51 (1995) 13337.
- [5] T.A. Burr, A.A. Seraphin, E. Werwa, K.D. Kolenbrander, Phys. Rev., B 56 (1997) 4818.
- [6] N.A. Hastas, C.A. Dimitriadis, D.H. Tassis, S. Logothetidis, Appl. Phys. Lett. 79 (2001) 638.
- [7] B.D. Weaver, P.E. Thompson, N. Jin, S.-Y. Chung, A.T. Rice, P.R. Berger, J. Appl. Phys. 95 (2004) 6406 (and references there in).
- [8] G.Y. Xu, M. Liu, T.M. Wang, J.L. Wang, Y.L. He, J. Phys., C: Condens. Matter 11 (1999) 8495.
- [9] D.V. Lang, J.D. Cohen, J.P. Harbison, Phys. Rev., B 25 (1982) 5285.
- [10] J.D. Cohen, D.V. Lang, Phys. Rev., B 25 (1982) 5321.
- [11] E. Kapetanakis, P. Normand, D. Tsoukalas, K. Beltsios, J. Stoemenos, S. Zhang, J. van den Berg, Appl. Phys. Lett. 77 (2000) 3450.
- [12] H. Fujiwara, M. Kondo, A. Matsuda, Phys. Rev., B 63 (2001) 115306.
- [13] P. Viktorovitch, D. Jousse, J. Non-Cryst. Solids 35/36 (1980) 569.
- [14] A.J. Snell, K.D. Mackenzie, P.G. Le Comber, J. Non-Cryst. Solids 35/36 (1980) 593.
- [15] T. Schmidt, R.J. Haug, K.V. Klitzing, Phys. Rev., B 55 (1997) 2230.
- [16] S.M. Sze, Physics of Semiconductor Devices, second edition, John Wiley & Sons, New York, 1981, chapter 9.
- [17] C. Rivas, J. Appl. Phys. 94 (2003) 5005.
- [18] A.G. Chynoweth, W.L. Feldmann, R.A. Logan, Phys. Rev. 121 (1961) 684.